



## Article

# Detecting a Sinistral Transpressional Deformation Belt in the Zagros

Mohammad Ali Ghanbarian <sup>1</sup>, Ali Yassaghi <sup>2</sup>  and Reza Derakhshani <sup>3,4,\*</sup> 

<sup>1</sup> Department of Earth Science, College of Science, Shiraz University, Shiraz 76147-13565, Iran; maghanbarian@shirazu.ac.ir

<sup>2</sup> Department of Geology, Tarbiat Modares University, Tehran 14115-175, Iran; yassaghi@modares.ac.ir

<sup>3</sup> Department of Geology, Shahid Bahonar University of Kerman, Kerman 76169-13439, Iran

<sup>4</sup> Department of Earth Sciences, Utrecht University, 3584CB Utrecht, The Netherlands

\* Correspondence: r.derakhshani@uu.nl

**Abstract:** The oblique collision between the northeastern margin of the Arabian platform and the Iranian microcontinent has led to transpressional deformation in the Zagros orogenic belt in the central part of the Alpine–Himalayan orogenic belt. Although previous articles have emphasized the dextral sense of shear in the Zagros orogenic belt, in this paper, using several indicators of kinematic shear sense upon field checking and microscopic thin-section studies, evidence of the development of a sinistral top-to-the NW deformation belt is presented. The mean attitudes of the foliations and lineations in this belt are 318°/55°NE and 19°/113°, respectively.

**Keywords:** transpression; shear sense; Sanandaj–Sirjan metamorphic belt; tectonics; Zagros; Iran



**Citation:** Ghanbarian, M.A.;

Yassaghi, A.; Derakhshani, R.

Detecting a Sinistral Transpressional Deformation Belt in the Zagros.

*Geosciences* **2021**, *11*, 226. <https://doi.org/10.3390/geosciences11060226>

Academic Editors: Rodolfo Carosi and Jesus Martinez-Frias

Received: 10 May 2021

Accepted: 20 May 2021

Published: 24 May 2021

**Publisher's Note:** MDPI stays neutral with regard to jurisdictional claims in published maps and institutional affiliations.



**Copyright:** © 2021 by the authors. Licensee MDPI, Basel, Switzerland. This article is an open access article distributed under the terms and conditions of the Creative Commons Attribution (CC BY) license (<https://creativecommons.org/licenses/by/4.0/>).

## 1. Introduction

From a tectonic point of view, Iran includes several geological zones, including the Zagros, Central Iran, Alborz, and the east and southeast of Iran, in some of which there are some sub-zones and belts such as Makran, Lut, Sistan suture zone, Urumieh–Dokhtar magmatic belt, and Sanandaj–Sirjan Zone (SSZ). Each of them is characterized by relatively unique recordings of magmatic activity, metamorphism, stratigraphy, orogenic events, and tectonic features. The Zagros orogenic belt is one of the largest areas on earth that has undergone transpressional deformation [1] and covers an area of about 700,000 km<sup>2</sup> in the central part of the Alpine–Himalayan orogenic system. Therefore, understanding the kinematics of the Zagros transpressional belt is important to constrain the tectonic development of this part of the Alpine–Himalayan orogenic system. This means that this orogen is one of the most studied and known collision belts [2–27]. This belt has been formed by NE-dipping subduction of Neo-Tethys under the Iranian microcontinent in the Jurassic to Paleogene followed by the subsequent oblique collision of the central Iran microcontinent and the Arabian platform in the Neogene (Figure 1) [2,28,29] where post-collisional crustal shortening is still active today [30–33]. Evidence of dextral transpressional deformation has been reported in previous studies [3], although there are various aspects of kinematics and complex deformation patterns across the belt that are not yet well understood. The fabric of Heneshk (Kowlikosh) shear zones (Figure 2 in [14]) and Neyriz area (Figure 3 in [1]) indicates the occurrence of sinistral deformation in the south-central part of the Zagros orogenic belt. Our study presents considerable evidence (140 km long and 20 km wide) of NW–SE striking sinistral top-to-the NW ductile and brittle–ductile shear belt in the central part of the Zagros orogenic belt [34–37]. The main purpose of this work is to investigate the structural development of a crustal-scale shear belt with sinistral top-to-the NW sense in the northeastern part of Fars province along the Zagros Hinterland Fold-and-Thrust Belt (ZHFTB; Figure 2).

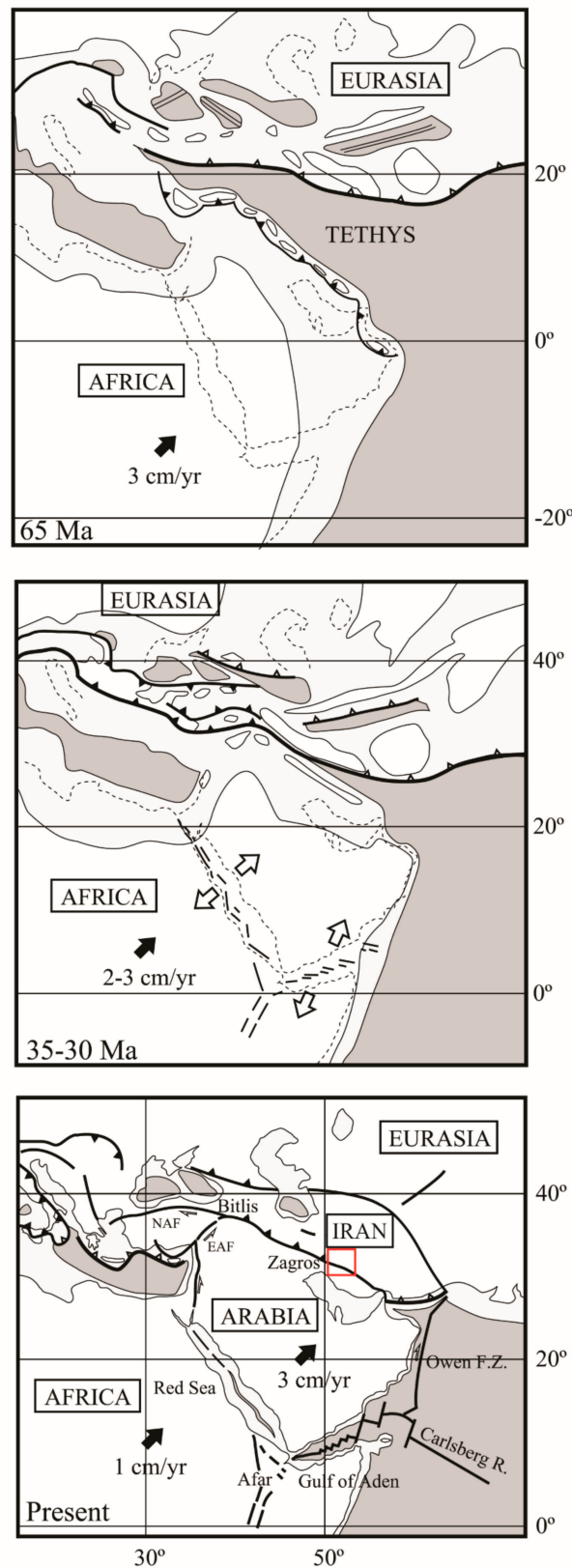


**Figure 1.** Cenozoic plate tectonic evolution of the Iranian, Arabian, NE African, and south of Eurasian plates, at 65, 35–30 Ma, and present-day ages (modified after [38]). Dark gray regions represent oceanic crusts and white regions represent continents. Empty arrows are the direction of extension. Black arrows are absolute velocities [39]. The red square in the present-day configuration of the plates shows the location of Figure 2b.



## 2. Geological Setting

The Zagros orogenic belt extends from the East Anatolian fault in the NW, to the Minab fault in the SE in an arid region, which forms well-exposed structures that are mainly the result of convergence between the Iranian and Arabian plates [2,28–33]. Three main episodes of convergence are involved, including the Cretaceous perturbation of subduction processes, the Paleocene–Eocene slab break-off with major shifts in arc magmatism, and the Oligocene–Quaternary collision and topographic build-up [7]. The main direction of ongoing shortening, according to GPS sites fixed in the central Iran microcontinent, is approximately north–south with an increase in convergence rate from  $4.5 \pm 2 \text{ mm yr}^{-1}$  in the northwest of Zagros to  $9 \pm 2 \text{ mm yr}^{-1}$  in the southeastern part of the belt [4]. The result of this long-standing and ongoing oblique convergence is the Zagros orogenic belt, which comprises five major sub-parallel tectonic elements. They are, from SW to NE, (1) the Zagros foreland folded belt, (2) the Zagros foreland fold-and-thrust belt [40,41], (3) the Sanandaj–Sirjan metamorphic belt (SSMB) [42], (4) the Zagros hinterland fold-and-thrust belt (ZHFTB) [41], and (5) the Urumieh–Dokhtar magmatic belt (Figure 2) [40]. The general tectonic vergence of all these belts is to the SW. The SSZ, with an approximate length of 1500 km and a width of 150 to 200 km, runs NW–SE, parallel to the high Zagros, and was first named by Stocklin [40]. It consists of the SSMB and the ZHFTB [43]. Compared to the high Zagros mountains, which are mostly sedimentary, this region has relatively low relief [44] and includes mainly high-pressure/low-temperature metamorphic and igneous rocks. The southwestern margin of SSZ is bounded by the Zagros thrust system and separates it from the Zagros foreland zone. Mohajjel [45] attributes the deformation recorded in the metamorphic rocks of the Sanandaj–Sirjan region to the subduction of the Neotethys oceanic crust beneath the continental blocks. The study area, located in the ZHFTB, is characterized by various kinds of ductile and brittle–ductile structures.

The Zagros orogenic belt consists of a Pan-African metamorphic basement covered by a thick Phanerozoic sequence [10]. The most important stratigraphic units of the Phanerozoic sequence which are exposed in the study area are: (1) Upper Silurian to Upper Devonian slate, phyllite, and meta-andesite; (2) Upper Devonian quartz arenite, shale, and marl; (3) Carboniferous grey, well-bedded, fetid limestone with a Visean quartz arenite unit in the lower part; (4) Permian light to dark grey well-bedded limestone with a distinct lower unit comprising brownish-red sandstone and shale; (5) Triassic dolomite, limestone, marl, and gypsum; (6) Lower Jurassic grey thin-bedded sandstone, shale, and siltstone; (7) Upper Jurassic thick-bedded to massive fetid oolitic limestone and conglomerate; (8) Lower Cretaceous thin- to medium-bedded limestone and dolomite; (9) Upper Oligocene–Lower Miocene thickly-bedded to massive limestone. Among these stratigraphic units, Permian limestone and marble form the most outcrops of the region and most of the shear zones of the study area occur in this unit. The Triassic thickly bedded dark brown dolomite has been metamorphosed to dolomarl up to greenschist facies conditions [14] in the southwestern part of Heneshk. The study area is characterized by different types of faults, completely different duplex structures in terms of size, macroscopic to microscopic fault-related folds [41], and well-developed ductile and brittle–ductile shear zones. The shear zones are intersected by a variety of faults (Figures 3a and 4a), most of which are NE-(hinterland-) dipping thrusts, but there are also some sinistral strike-slip faults in the Faryadoun, Kuh-e-Sefid, Sourmagh, and Abadeh area (Figures 3 and 4) that have displaced rock units up to about 600 m.

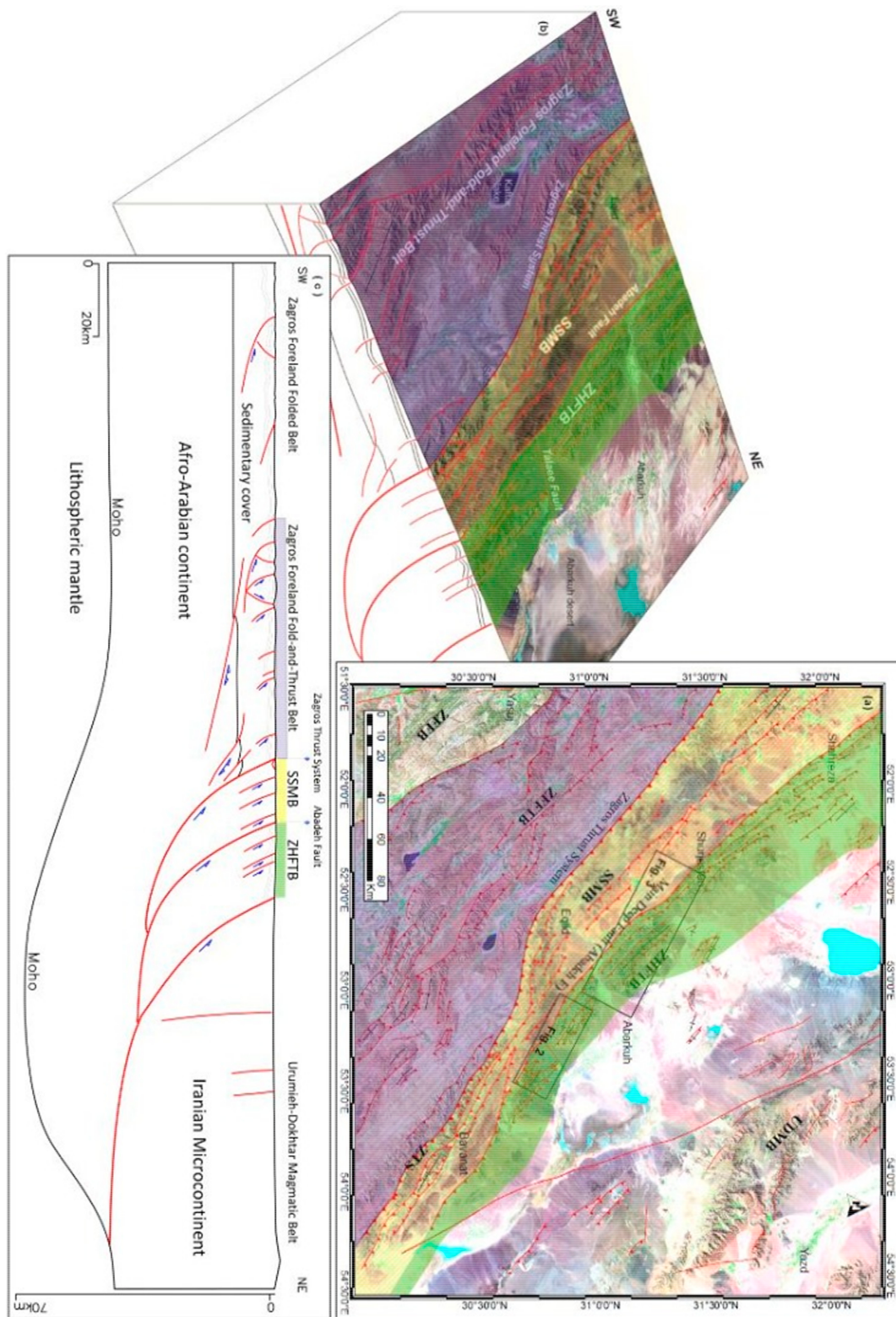


**Figure 2.** (a) Satellite image (from MrSID, Multi-resolution Seamless Image Database) showing the main structures of the study area and the main subdivisions of the central part of the Zagros collision belt near the Zagros thrust system; (b) Crustal-scale block diagram of the central part of the Zagros collision belt; (c) A schematic cross-section of Zagros showing its structural zones. The depth of Moho is adapted from [9] and the depth of the basement in the Afro-Arabian continent is adapted from [11]. The structures of the Zagros foreland fold-and-thrust belt and Zagros foreland folded belt are adapted from [46–50].

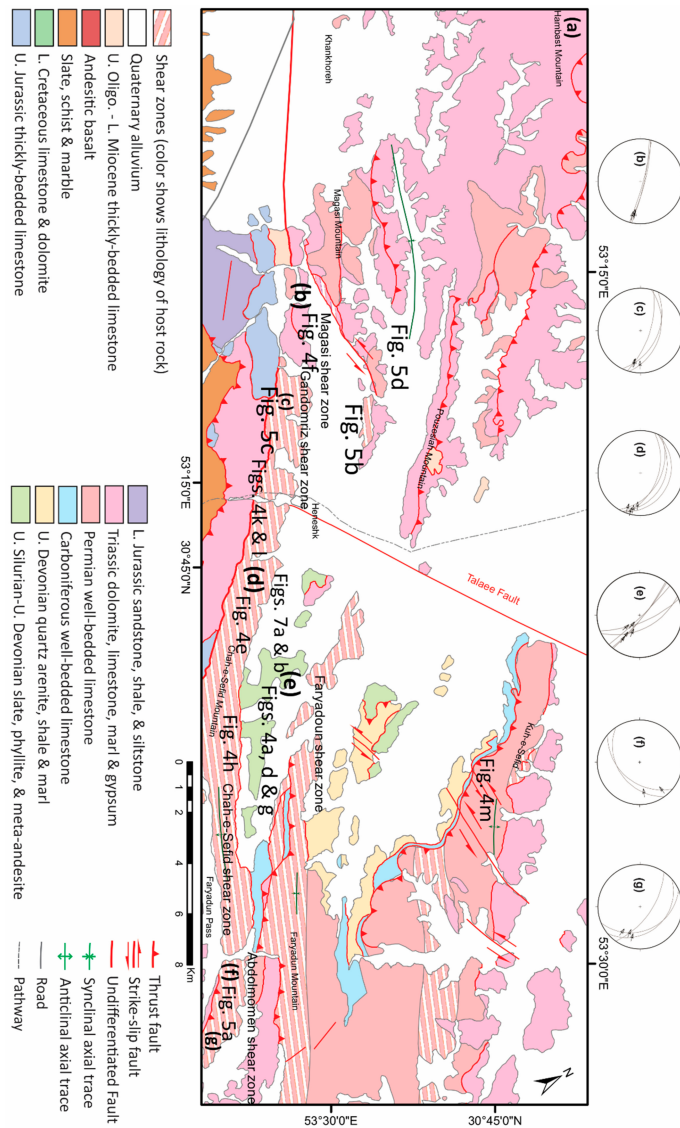


**Figure 3.** (a) Geological map of the SE of the study area, modified after [37], (b–g) Stereographic projection from the lower hemisphere showing the orientation of the foliations, stretching lineations, and the shear senses of the Magasi (b), Gandomriza (c), Chah-e-Sefid [43] (d), Faryadun [43] (e), Abdolmomen 1 (f), and Abdolmomen 2 (g) shear zones, respectively.

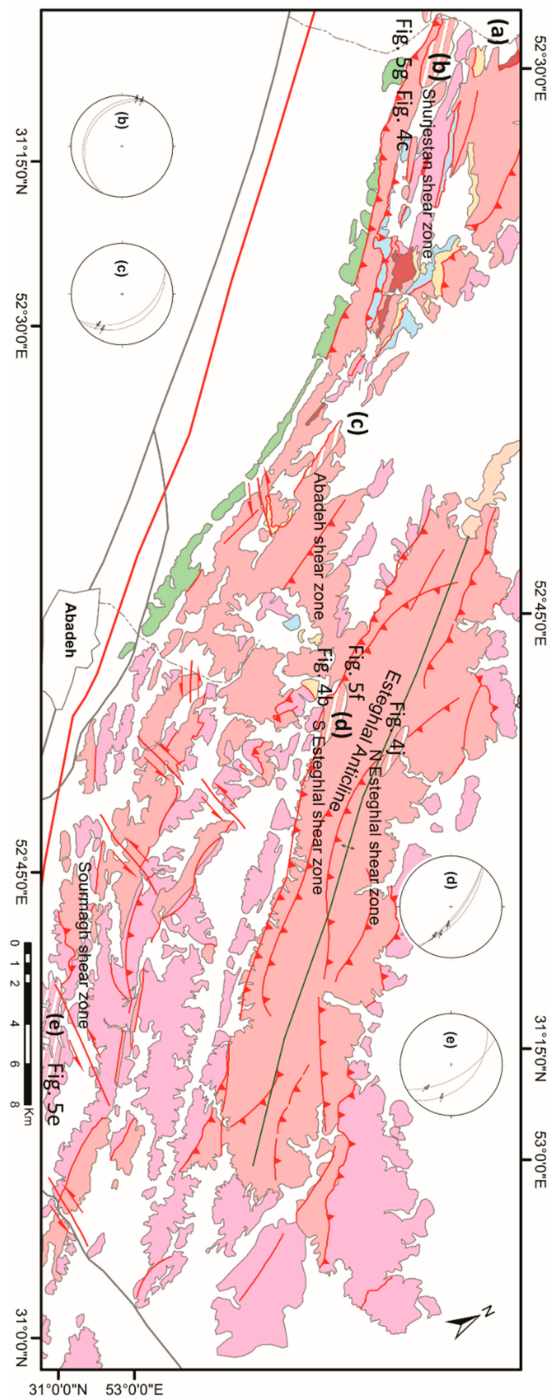


**Figure 4.** (a) The geological map of the NW of the study area, modified after [37]. The legend is the same as Figure 3; (b–e) Stereographic projection from the lower hemisphere showing the orientation of the foliations, stretching lineations, and the shear senses of the Shurjestan (b), Abadeh (c), South Esteghlal (d), and Sourmagh (e) shear zones, respectively.

### 3. Methodology

To study the structural characteristics and deformation pattern of the region, after considering the previous geological maps of the study area [51–53] and the Quickbird satellite images (Google Earth), several field works were performed in the different parts of the study area. Based on the satellite images and the field data, two simplified geostructural maps were prepared (Figures 3 and 4). During the field studies, important kinematic evidence such as fabrics of the shear zones and shear sense indicators like duplex structures,



asymmetric boudins, shear band type fragmented porphyroclasts, mesoscopic asymmetric folds, rotated mantled porphyroclasts and winged inclusions were recorded and analyzed. Several thin sections from the XZ-plane (perpendicular to the foliation and parallel to the lineation) of some of the important oriented samples have been studied under the microscope. Strain fringes and shear band cleavage are the most typical microscopic shear sense indicators that have been studied. The main purpose of considering these structures is to study the sense of flow in the observed shear zones. Because kinematic indicators, such as asymmetric folds and even rotated porphyroclasts, cannot be used as single structures, the fabric elements of the shear zones and many mesoscopic and microscopic shear sense indicators are considered together.

#### 4. Shear Zones of the Area

The shear zones of the study area are in the range of meters to hundreds of meters in thickness and exposed in the different parts of the ZHFTB (Figures 3 and 4). Shear zones were developed in the Permian slightly metamorphosed limestone unit and formed calcite mylonite, apart from the Sourmagh shear zone which has developed in the Triassic limestones. No shear zones have been detected in the younger units of the study area. The main minerals of the shear zones are calcite, dolomite, ankerite, quartz, chert, chlorite, sericite, and pyrite. The shear zones are NW- to WNW directed by NE-dipping, parallel to the structural trend of the Zagros orogenic belt, except for the Abdolmomen 1 (Figure 3f) and Shurjestan (Figure 4b) shear zones which dipped toward SW and SE, respectively. The strike of foliations in the Magasi, Gandomriz, Chah-e-Sefid, Faryadoun, Abdolmomen 2, Abadeh, South Esteghlal, North Esteghlal, and Sourmagh shear zones varies between N20° W to N75° W (average: N48° W) and their dips range between 20° to 80° NE (average: 55°) (Figures 3 and 4). Their mineral lineations (Figure 5a,b) are horizontal to moderately plunging to the SE (average: 19°/113°) (Figures 3 and 4). Moreover, many mesoscopic and microscopic kinematic indicators are developed in these shear zones. The most important kinematic indicators are rotated porphyroclasts, winged inclusions, strain fringes, shear band cleavage, sigmoid objects, asymmetric boudins, asymmetric folds, and duplex structures (Figures 5, 6 and 8).

##### 4.1. Outcrop Scale Structures in the Shear Zones

###### 4.1.1. Rotated Mantled Porphyroclasts and Winged Inclusions

Many typical rotated inclusions and mantled porphyroclasts (Figure 5c–f) have been observed in the several shear zones of the area which have developed in the Permian metalimestones and the Middle Triassic thickly-bedded dolomite (e.g., Faryadoun, Chah-e-Sefid, Shurjestan, and Magasi shear zones). Evidence of porphyroclasts' or inclusions' rotations and their senses at these microscopic- to mesoscopic-scales is very clear. Most of the porphyroclasts are made of carbonate minerals such as dolomite and ankerite, which are highly competitive compared to schist, phyllite, and calcite mylonite matrices.

###### 4.1.2. Duplex Structures

The presence of multiple duplexes at different scales is a feature of this region, while macroscopic brittle thrust duplex structures have formed the structural architecture of the region [41], microscopic and mesoscopic transpressive duplexes have developed with shear sense related to the kinematic properties of the ductile shear zones. In the Faryadoun shear zone, for example, a 30 cm long, E-dipping, fault-bounded horse with ramps that transfer displacements from a lower E-dipping limb wedge thrust to an upper subparallel out-of-syncline thrust has been observed (Figure 5g). Another example is a small NW verging duplex structure in the grey marbles of the Chah-e-Sefid shear zone (Figure 5h). They clearly show the sense of shearing in their ductile shear zones (i.e., Faryadoun and Chah-e-Sefid shear zones).

#### 4.1.3. Asymmetric Boudins

There are widespread asymmetric boudins at different scales in the shear zones of the different parts of the region. They are usually quartzitic boudins that have high competency in comparison with the enveloping layers of calcite tectonites of the shear zones such as the Chah-e-Sefid, and Esteghlal shear zones (Figure 5j–m). These shear zones have been developed in the Permian dolomarmbles and metacarbonates. Most of the boudins are curvilinear, lens-shaped, and with a moderate aspect ratio. They have synthetic drags on the inter-boudin surfaces in which their asymmetrical shapes are related to synthetic slip between boudins. They are known as shear band boudins based on the classification of Goscombe [54].

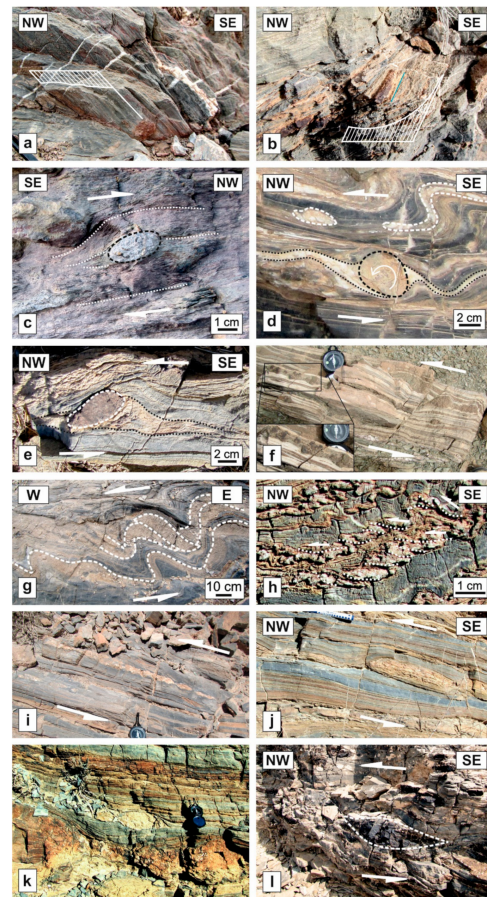


**Figure 5.** (a) Field photographs of foliation and lineation of the Faryadun shear zone [43]; (b) Foliation and lineation of the SW of the Esteghlal shear zone; (c) A calcite porphyroclast in schists of top-to-the NW Shurjestan shear zone; (d) Mesoscopic ankerite porphyroclasts in the XZ-plane of the calcite mylonites of the Faryadun shear zone with its light calcite mantle showing counter-clockwise rotation [34]; (e) A sinistrally rotated mesoscopic porphyroclasts in the XZ-plane of the Chah-e-Sefid shear zone [34]; (f) Mesoscopic porphyroclasts (left of the photograph) and shear band type fragmented porphyroclast (right of the photograph) in the XZ-plane of the Magasi shear zone which shows sinistral top-to-the NW deformation. The compass needle is 55 mm long and toward N; (g) S-shaped asymmetric folds and a mesoscopic duplex structure which have been produced by out-of-syncline and limb wedge thrusting in the XZ-plane of the sinistral top-to-the NW Faryadun shear zone [34]; (h) Mesoscopic duplex structure and asymmetric folds in the Chah-e-Sefid shear zone [43]; (i) Shearband quartzitic boudins in the North Esteghlal shear zone; (j) Shearband quartzitic boudins in the Chah-e-Sefid shear zone [34]; (k) Asymmetric boudins in the Chah-e-Sefid shear zone; (l) Asymmetric boudins in the Kuh-e-Sefid shear zone. See Figures 3 and 4 for their locations.



#### 4.1.4. Shear Band Type Fragmented Porphyroclasts

There are some more rigid porphyroclasts compared to the enveloping layers which have been fragmented during the deformation in the shear zones of the study area. In terms of composition, porphyroclasts are usually ankerite and dolomite in the calcite matrices and structurally, these porphyroclasts have been separated into aggregates of fragments with geometric like shear band boudins. For example, in the Magasi shear zone (Figure 3), there are mesoscopic ankerite shear band type fragmented porphyroclasts in light-colored layers of calcite mylonite (as matrix) (Figure 5h).

#### 4.1.5. Mesoscopic Asymmetric Folds

In this region, folds can be seen at different scales, from fault-related folds at the map scale to asymmetric folds at the outcrop scale (Figure 6). The amplitudes of the shear zones' asymmetric folds vary between one centimeter to several meters. These structures are composed of chert, dolomite, and ankerite layers which are usually more rigid than the enveloping layers of schists, metasandstones, and calcite mylonites. While map-scale asymmetric fault-related folds of the area play an important role in the architecture of the region, very abundant mesoscopic asymmetric folds in the shear zones can help to constrain the kinematics of the region. These outcrop-scale structures have distinct vergences which can be used for determining the sense of shear.

### 4.2. Microscopic Structures in the Shear Zones

#### 4.2.1. Strain Fringes

In microscopic studies of the shear zones of the study area, some typical strain fringes have been observed in the Chah-e-Sefid shear zone. The main minerals in the fringes are quartz, chlorite, and muscovite which occur adjacent to pyrite grains. The growth surface is between the core (pyrite grain) and the fringes; therefore, they are typically antitaxial based on the classification of Passchier and Trouw [55] or pyrite-type fringes based on the classification of Ramsay and Huber [56]. The fiber growth in fringes shows that these structures can be classified as displacement-controlled fringe structures (Figure 7a). The overall shapes of these microscopic structures in the XZ-plane of the Chah-e-Sefid shear zone resemble the letter Z which can be used to deduce the sense of shear.

#### 4.2.2. Shear Band Cleavage

The preferred orientation of compositional layers of muscovites and chlorites within deformed rocks of the Chah-e-Sefid shear zone has been cut by sets of subparallel smaller shear bands at a small angle (Figure 7b). These structures, known as shear band cleavage [57–61], are classified as  $C'$ -type (Based on the Berthé classification [62] since the cleavages are oblique to shear zone boundaries (15–35°) and to the older foliation. These  $C'$ -type shear band cleavages in the study area are consistent with other shear sense indicators in the shear zones of the study area (Figure 7b).

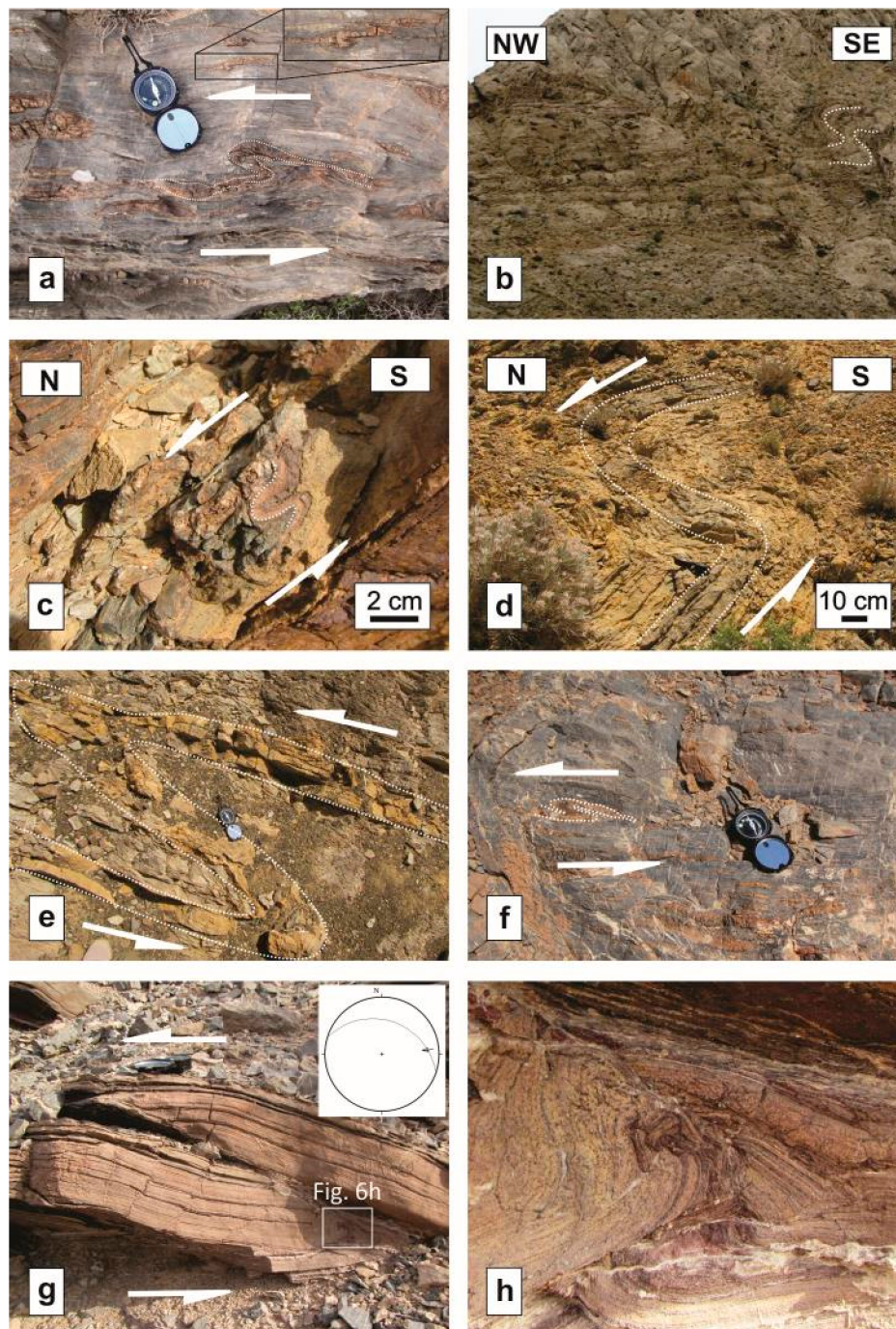


**Figure 6.** (a) A sinistral ptygmatic fold in a chert layer in the metamorphosed Permian limestones of the Abdolmomen 2 shear zone; (b) An asymmetric fold highlighted by brown chert layers which suggest sinistral top-to-the NW sense of shear; (c) An outcrop-scale asymmetrical fold in the dolomitic limestone layers; (d) A mesoscopic sinistral asymmetric fold in the Middle Triassic thickly-bedded dark brown dolomite; (e) A mesoscopic sinistral top-to-the NW asymmetric fold in the Lower Triassic marl and limestone unit of the Sourmagh shear zone; (f) A sinistral ptygmatic fold in a chert layer in the metamorphosed Permian limestones of the Abadeh shear zone; (g) A mesoscopic top-to-the W thrust in the well-bedded limestones and dolomites. The inset presents stereographic projection from the lower hemisphere showing the orientation of the foliation, stretching lineation, and the sense of shear; (h) A mesoscopic thrust-related asymmetric fold that suggests a top-to-the W sense of shear. The open compasses without fold-out pointers are 15 cm long and the fold-out pointers are toward N (a,e,f,g).



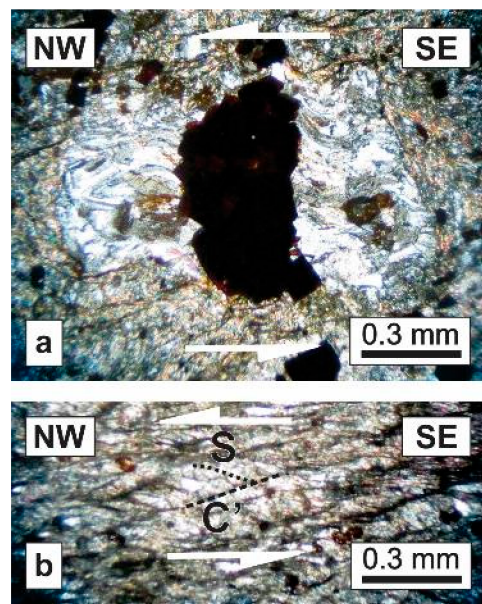


**Figure 7.** Sinistral top-to-the NW strain fringes of quartz and chlorite adjacent to an inequidimensional pyrite grain (a) and sinistral top-to-the NW C'-type shear bands cleavage (b) in the XZ-planes of the calcite tectonites in the Chah-e-Sefid shear zone [34]. The antitaxial fringe structure is displacement controlled (a).

## 5. Discussion

All of the shear sense indicators that have been utilized in this study are reliable and have already been studied by many scientists. The shear sense of deformation controls the geometry of the rotated or fragmented porphyroclasts; therefore, they can be utilized as a shear sense indicator [55,63]. Duplex structures, which are very common in collisional orogens [64–68], have been used as shear sense indicators by several authors [69–72]. Boudins, which can form at all scales and in all terranes under an extremely broad span of temperature, pressure, and fluid conditions, can afford significant information about the sense of shear, rheological properties, and the forces involved in tectonic deformation [73]. In addition, by using the internal and external shape of strain fringes, a lot of kinematic information can be obtained [74–76]. Shear band cleavages are also reliable shear sense indicators [60,61].

The use of asymmetric folds as shear sense indicators is arguable and not always misleading [72,77,78]. They should be used with careful consideration of several parameters due to the fact that some asymmetric folds verge in the direction opposite to the sense of shear [79,80]. The following are some different folding models that cause asymmetric folds with an opposite vergence to the sense of shear: (1) In simple shear folding with the original layer at an acute angle to the axial planes, increasing strain can result in apparently inconsistent vergence with the sense of shear (Figure 8a) [81,82]; (2) If a layer was at a low angle (Figure 8b) [83] or a high angle (Figure 8c) [79] relative to the axial plane, heterogeneous simple shear with a constant sense of shear parallel to the axial plane constructs folds that verge in the direction opposite to the sense of shear; (3) If the orientation of the layer, before folding, is perpendicular to the maximum shear stress, the shear sense is the reverse of what is inferred from the folds due to reversal of shear sense across the axial plane in heterogeneous simple shear parallel to the axial plane (Figure 8d) [84]. In all these cases, the initial orientations of the folded layers are not parallel to the maximum shear stress. However, the folded layers were considered as shear sense indicators in this study in which the initial orientation of the layers are subparallel to the maximum shear stress and the asymmetric folds, which are very well distributed at various development stages in samples (Figure 6). Moreover, asymmetric folds are associated with examples of more reliable shear sense indicators such as rotated porphyroclasts and duplex

structures (Figure 5d,g,h). Therefore, it can be concluded that none of the asymmetric folds investigated in this study verged in the direction opposite to the sense of shear.

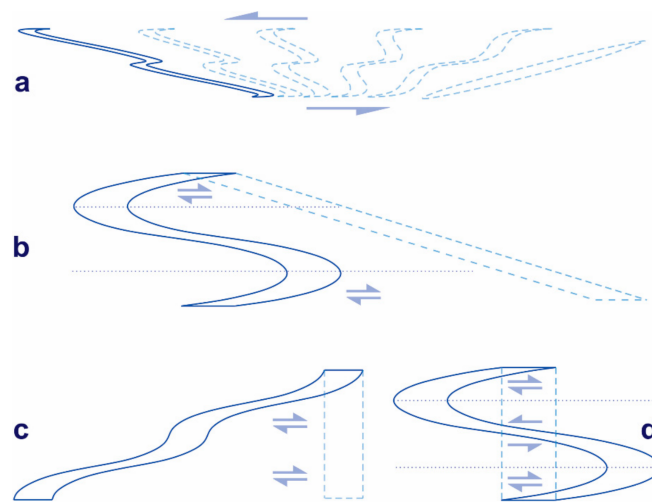


**Figure 8.** Four different models of folding create asymmetric folds that show opposite vergence of the sense of shear: (a) Increasing strain (to the left in this figure) when the initial layer is at a low angle to axial plane in simple shear folding [81,82]; (b) Initial layer at a low angle to axial plane, heterogeneous simple shear with a constant sense of shear parallel to the axial plane [83]; (c) Initial layer at a right angle to axial plane, asymmetric folds produced by heterogeneous simple shear with a constant sense of shear parallel to the axial plane [79]; (d) Initial layer at a right angle to axial plane, heterogeneous simple shear parallel to axial plane, reversal of shear sense across axial plane [84].

All of these observed reliable shear sense indicators of the study area have been analyzed in the XZ-plane of the strain ellipsoid of the shear zones (i.e., parallel to the stretching lineation and perpendicular to the foliation). In transpression, only a few objects rotate against shearing direction due to the component of pure shear [85], but other objects do not rotate in an opposite sense concerning the main sense of shear. The attitudes of fabrics and all the studied shear sense indicator structures of the moderately-dipping Gandomriz (Figure 3c), Chah-e-Sefid (Figure 3d), Abdolmomen 2 (Figure 3g), Abadeh (Figure 4c), and Sourmagh (Figure 4e) shear zones show sinistral top-to-the NW senses of shear. The attitudes of fabrics and the studied shear sense indicators of the steeply-dipping Magasi (Figure 3b), Faryadoun (Figure 3e), and Esteghlal (Figure 4d) shear zones show sinistral senses of shear. The sub-horizontal Shurjestan (Figure 4b) and SE-dipping Abdolmomen 1 (Figure 3f) shear zones are top-to-the NW and sinistral top-to-the WSW, respectively. All these mentioned shear senses are in contradiction with what is known so far for the central part of the Zagros collision belt. The spatial distribution of the structures that represent these senses of shear is extensive, and to the best of our knowledge, can be detected, at least from north of Shurjestan to the north of Bavanat in a 140 km long belt with an area of 2500 km<sup>2</sup> (Figure 2). There is no evidence of dextral deformation and 90% of the shear zones are NW-striking (parallel to the Zagros belt). On the other hand, the mineral assemblages suggest that these sinistral shear zones developed under lower P-T conditions with respect to the previously-known dextral transpression in the northern SSZ [3]. Therefore, they cannot be interpreted as conjugate Riedels of a main dextral deformation. This sense of shear cannot be also attributed to a possible block rotation due to the consistency of the structures (e.g., thrust faults and fault-related folds). In addition, there is a wide range in the dips of the shear zones that rejects the hypothesis of the existence of block rotation. There are many other assumptions that relate to the occurrence of this sinistral top-to-the NW belt; one of them is the occurrence of shearing motions with opposite sense of shear in the flanks of larger-scale antiforms as reported from the gneiss, amphibolite, and migmatite of the Neyriz area [86]. Investigation of geometric

relations and kinematic analysis of structures indicating the sense of shearing refutes the above hypothesis about the study area in the present research. The low-plunge large-scale folds of the region and low-plunge lineations in the all observed shear zones in the different parts of the study area such as Gandomriz, Magasi, Chah-e-Sefid, Faryadoun, Abadeh, Shurjestan, and Esteghlal shear zones indicate that these shear zones are not related to the shearing motions in the flanks of folds. The tectonic architecture of the area, which has been described by Sarkarinejad and Ghanbarian [41], is in contrast with this model.

The vertical to sub-vertical shear belts with opposite sense of shear can be developed due to the progressive bending of the arc in western Yunnan (China) [87], or because of the curvature in the boundary between the Iranian microcontinent and Arabian platform in the southeasternmost part of Zagros [88]. There is not, however, a curvature or bending between the study area and the study area of Mohajjel and Fergusson [3] and the shallow to moderate dips of most of the shear zones are not consistent with that models [87,88].

This sinistral top-to-the NW belt also may be assumed to be related to the Doruneh fault system's slip-sense inversion. The slip-sense of this major basement fault has changed from Early Eocene to Late Miocene right-lateral movement to post-Early Pleistocene left-lateral motions [89]. The Doruneh strike-slip movements rotate the Central Iran microcontinent. The post-Early Pleistocene clockwise rotation of the Central Iran microcontinent, however, is too young to form this exhumed sinistral ductile shear belt.

The influence of a major inferred dextral NW–SE trending fault in the NE of the ZHFTB [90], and tectonic inversion [43] are the other possible models for the development of this unexpected flow sense belt. However, a change in the direction of the regional stress field [34–36] is another probable scenario that has been proved in the other adjacent regions. For example, it has been reported from the southeasternmost part of Zagros orogen [32], central Zagros foreland fold-and-thrust belt [91], Fars Province [1,16], and W-Zagros [18]. Considering the currently active direction of shortening is roughly N–S [4], which is compatible with the current dextral sense of shear in the Zagros NW–SE trending belt, this indicates that the sinistral top-to-the NW shearing is due to an older deformational phase. The formation of this sinistral top-to-the NW belt may have resulted from a relative rotation in the direction of the regional shortening during the long convergence history of the Iranian microplate and Afro-Arabian continent. The relative rotation in the direction of the regional shortening could be in turn reflecting the relative rotation of the convergence direction concerning the Iranian microcontinent's and the Arabian platform's boundaries throughout continental convergence. This phenomenon may be due to counterclockwise rotation of the stress ellipsoid or clockwise rotation of the orientation of the continental blocks' boundaries through the continental convergence or both of these processes occurring. Although the present-day convergence vector of the region is about N–S [4], considering that the paleo-orientations of the plate boundaries were the same as now (i.e., N125°), in the time of the development of the sinistral and top-to-the NW structures, the maximum principal stress ( $\sigma_1$ ) axis was directed toward NE–SW (i.e., with an azimuth more than N035°; Figure 9). According to Navabpour et al. [12,13], in the Zagros collisional belt, the azimuth of  $\sigma_1$  stress axes in the Early Miocene was N053°. Assuming that the paleo-orientations of the plate borders were similar as at the present, the direction of the  $\sigma_1$  stress axis was suitable in the Early Miocene for the development of the sinistral top-to-the NW belt. In the Early Miocene, the Neo-Tethys oceanic lithosphere was subducting beneath the Iranian continental microplate [15]. The development of such an intensely deformed belt indicates strong mechanical coupling of the two plates (Chile-type or forced subduction).

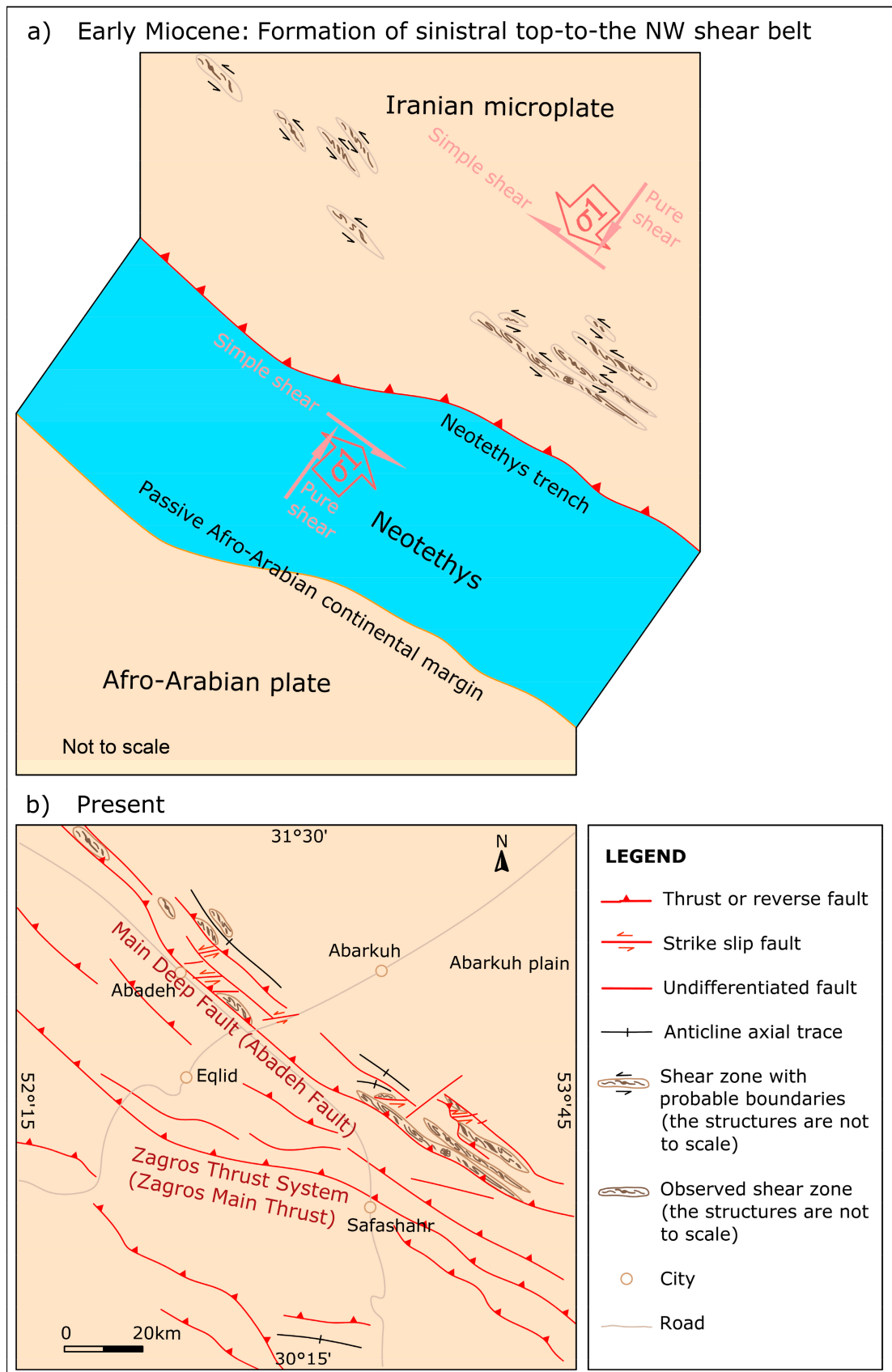


**Figure 9.** Diagrams showing the plate tectonic evolution of the study area. (a) The development of the sinistral top-to-the NW shear belt in the Early Miocene; (b) The present situation.



The relative rotation of the regional shortening model is also compatible with the work of McQuarrie et al. [92]. This study has shown the rotation of the convergence direction of Africa and Arabia with respect to Eurasia which was constructed based on positions of seafloor magnetic anomalies and fracture zones in the North and Central Atlantic [93–95] and reconstructions across the Red Sea [96]. Their reconstructed paths of relative Arabia–Eurasia converging motion included a shift in average values from N030° in the 56–33 Ma to N025° in the 33–19 Ma, N009° in the 19–10 Ma, and N005° in the last 10 Ma.

## 6. Conclusions

The attitudes of fabrics (average foliation: 318°, 55° NE, and average lineation: 19°/113°) and the shear sense indicators of all of the shear zones (rotated porphyroclasts, strain fringes, duplex structures, asymmetric boudins, fragmented porphyroclasts, asymmetric folds, and shear band cleavages) in the studied part of ZHFTB show sinistral, top-to-the NW, and sinistral top-to-the NW senses of shear in the vertical, horizontal, and oblique shear zones, respectively.

This long shear belt is parallel to the general trend of the Zagros belt and cannot be developed as conjugate Riedels of a main dextral deformation, or due to the shearing motions with opposite sense of shear in the flanks of larger-scale antiforms as well as due to curvature or bending of the belt.

A change in the direction of the regional stress field is a possible scenario for the development of this belt and is compatible with the many previous studies, but we must first examine the existence of such evidence in other parts of Sanandaj–Sirjan, which is beyond the scope of these studies due to its vastness, and further studies in this area are recommended.

**Author Contributions:** Conceptualization, M.A.G.; methodology, M.A.G.; A.Y.; software, R.D.; M.A.G.; validation, M.A.G.; formal analysis, M.A.G.; A.Y.; investigation, M.A.G.; resources, M.A.G.; R.D.; data curation, M.A.G.; writing—original draft preparation, M.A.G.; A.Y.; writing—review and editing, M.A.G.; R.D.; visualization, M.A.G.; A.Y.; supervision, R.D.; A.Y.; project administration, M.A.G.; R.D. All authors have read and agreed to the published version of the manuscript.

**Funding:** This research received no external funding.

**Conflicts of Interest:** The authors declare no conflict of interest.

## References

1. Sarkarinejad, K.; Faghih, A.; Grasemann, B. Transpressional deformations within the Sanandaj-Sirjan metamorphic belt (Zagros Mountains, Iran). *J. Struct. Geol.* **2008**, *30*, 818–826. [[CrossRef](#)]
2. Mohajjel, M.; Fergusson, C. Jurassic to Cenozoic tectonics of the Zagros Orogen in northwestern Iran. *Int. Geol. Rev.* **2013**, *56*, 263–287. [[CrossRef](#)]
3. Mohajjel, M.; Fergusson, C.L. Dextral transpression in Late Cretaceous continental collision, Sanandaj-Sirjan Zone, western Iran. *J. Struct. Geol.* **2000**, *22*, 1125–1139. [[CrossRef](#)]
4. Vernant, P.; Nilforoushan, F.; Hatzfeld, D.; Abbassi, M.R.; Vigny, C.; Masson, F.; Nankali, H.; Martinod, J.; Ashtiani, A.; Bayer, R.; et al. Present-day crustal deformation and plate kinematics in the Middle East constrained by GPS measurements in Iran and northern Oman. *Geophys. J. Int.* **2004**, *157*, 381–398. [[CrossRef](#)]
5. McQuarrie, N. Crustal scale geometry of the Zagros fold-thrust belt, Iran. *J. Struct. Geol.* **2004**, *26*, 519–535. [[CrossRef](#)]
6. Agard, P.; Omrani, J.; Jolivet, L.; Mouthereau, F. Convergence history across Zagros (Iran): Constraints from collisional and earlier deformation. *Acta Diabetol.* **2005**, *94*, 401–419. [[CrossRef](#)]
7. Agard, P.; Omrani, J.; Jolivet, L.; Whitechurch, H.; Vrielynck, B.; Spakman, W.; Monie, P.; Meyer, B.; Wortel, R. Zagros orogeny: A subduction-dominated process. *Geol. Mag.* **2011**, *148*, 692–725. [[CrossRef](#)]
8. Agard, P.; Monié, P.; Gerber, W.; Omrani, J.; Molinaro, M.; Meyer, B.; Labrousse, L.; Vrielynck, B.; Jolivet, L.; Yamato, P. Transient, synobduction exhumation of Zagros blueschists inferred from P-T, deformation, time, and kinematic constraints: Implications for Neotethyan wedge dynamics. *J. Geophys. Res. Space Phys.* **2006**, *111*. [[CrossRef](#)]
9. Paul, A.; Kaviani, A.; Hatzfeld, D.; Vergne, J.; Mokhtari, M. Seismological evidence for crustal-scale thrusting in the Zagros mountain belt (Iran). *Geophys. J. Int.* **2006**, *166*, 227–237. [[CrossRef](#)]
10. Alavi, M. Structures of the Zagros fold-thrust belt in Iran. *Am. J. Sci.* **2007**, *307*, 1064–1095. [[CrossRef](#)]
11. Mouthereau, F.; Tensi, J.; Bellahsen, N.; Lacombe, O.; De Boisgrollier, T.; Kargar, S. Tertiary sequence of deformation in a thin-skinned/thick-skinned collision belt: The Zagros Folded Belt (Fars, Iran). *Tectonics* **2007**, *26*. [[CrossRef](#)]

12. Navabpour, P.; Angelier, J.; Barrier, E. Cenozoic post-collisional brittle tectonic history and stress reorientation in the High Zagros Belt (Iran, Fars Province). *Tectonophysics* **2007**, *432*, 101–131. [[CrossRef](#)]
13. Navabpour, P.; Angelier, J.; Barrier, E. Stress state reconstruction of oblique collision and evolution of deformation partitioning in W-Zagros (Iran, Kermanshah). *Geophys. J. Int.* **2008**, *175*, 755–782. [[CrossRef](#)]
14. Sarkarinejad, K.; Azizi, A. Slip partitioning and inclined dextral transpression along the Zagros Thrust System, Iran. *J. Struct. Geol.* **2008**, *30*, 116–136. [[CrossRef](#)]
15. Arfania, R.; Shahriari, S. Role of southeastern Sanandaj-Sirjan Zone in the tectonic evolution of Zagros Orogenic Belt, Iran. *Isl. Arc* **2009**, *18*, 555–576. [[CrossRef](#)]
16. Aubourg, C.; Smith, B.; Eshraghi, A.; Lacombe, O.; Authemayou, C.; Amrouch, K.; Bellier, O.; Mouthereau, F. New magnetic fabric data and their comparison with palaeostress markers in the Western Fars Arc (Zagros, Iran): Tectonic implications. *Geol. Soc. Lond. Spéc. Publ.* **2010**, *330*, 97–120. [[CrossRef](#)]
17. Vergés, J.; Saura, E.; Casciello, E.; Fernandez, M.; Villaseñor, A.; Jiménez-Munt, I.; García-Castellanos, D. Crustal-scale cross-sections across the NW Zagros belt: Implications for the Arabian margin reconstruction. *Geol. Mag.* **2011**, *148*, 739–761. [[CrossRef](#)]
18. Navabpour, P.; Barrier, E. Stress states in the Zagros fold-and-thrust belt from passive margin to collisional tectonic setting. *Tectonophysics* **2012**, *581*, 76–83. [[CrossRef](#)]
19. Ghanbarian, M.A. Structural analysis of the Konarsiah and the Mangerak salt domes and its influence in ground water contamination, Zagros foreland folded belt, SW Iran. *Int. J. Environ. Sci.* **2016**, *7*, 70–82. [[CrossRef](#)]
20. Malekzade, Z.; Bellier, O.; Abbassi, M.R.; Shabani, E.; Authemayou, C. The effects of plate margin inhomogeneity on the deformation pattern within west-Central Zagros Fold-and-Thrust Belt. *Tectonophysics* **2016**, *693*, 304–326. [[CrossRef](#)]
21. Angiboust, S.; Agard, P.; Glodny, J.; Omrani, J.; Oncken, O. Zagros blueschists: Episodic underplating and long-lived cooling of a subduction zone. *Earth Planet. Sci. Lett.* **2016**, *443*, 48–58. [[CrossRef](#)]
22. Ghanadian, M.; Faghih, A.; Grasemann, B.; Fard, I.A.; Maleki, M. Analogue modeling of the role of multi-level decollement layers on the geometry of orogenic wedge: An application to the Zagros Fold-Thrust Belt, SW Iran. *Acta Diabetol.* **2017**, *106*, 2837–2853. [[CrossRef](#)]
23. Bayet-Goll, A.; Esfahani, F.S.; Daraei, M.; Monaco, P.; Sharafi, M.; Mohammadi, A.H. Cyclostratigraphy across a Mississippian carbonate ramp in the Esfahan-Sirjan Basin, Iran: Implications for the amplitudes and frequencies of sea-level fluctuations along the southern margin of the Paleotethys. *Acta Diabetol.* **2018**, *107*, 2233–2263. [[CrossRef](#)]
24. Rad, J.R.; Derakhshani, R.; Farhoudi, G.; Ghorbani, H. Basement Faults and Salt Plug Emplacement in the Arabian Platform in Southern Iran. *J. Appl. Sci.* **2008**, *8*, 3235–3241. [[CrossRef](#)]
25. Derakhshani, R. Existence of the Oman Line in the Empty Quarter of Saudi Arabia and its Continuation in the Red Sea. *J. Appl. Sci.* **2005**, *5*, 745–752. [[CrossRef](#)]
26. Rahnamarad, J.; Farhoudi, G.; Ghorbani, H.; Habibimood, S.; Derakhshani, R. Pierced salt domes in the Persian Gulf and in the Zagros mountain ranges. *Iran. J. Earth Sci.* **2009**, *1*, 57–72.
27. Mehrabi, A.; Dastanpour, M.; Radfar, S.; Vaziri, M.; Derakhshani, R. Detection of fault lineaments of the Zagros fold-thrust belt based on Landsat imagery interpretation and their relationship with Hormuz series salt dome locations using GIS analysis. *Geosciences* **2015**, *24*, 17–32. [[CrossRef](#)]
28. Rashidi, A.; Khatib, M.M.; Nilfouroushan, F.; Derakhshani, R.; Mousavi, S.M.; Kianimehr, H.; Djamour, Y. Strain rate and stress fields in the West and South Lut block, Iran: Insights from the inversion of focal mechanism and geodetic data. *Tectonophysics* **2019**, *766*, 94–114. [[CrossRef](#)]
29. Rashidi, A.; Abbassi, M.-R.; Nilfouroushan, F.; Shafiei, S.; Derakhshani, R.; Nemati, M. Morphotectonic and earthquake data analysis of interactional faults in Sabzevaran Area, SE Iran. *J. Struct. Geol.* **2020**, *139*, 104147. [[CrossRef](#)]
30. Talebian, M.; Jackson, J. Offset on the Main Recent Fault of NW Iran and implications for the late Cenozoic tectonics of the Arabia-Eurasia collision zone. *Geophys. J. Int.* **2002**, *150*, 422–439. [[CrossRef](#)]
31. Allen, M.B.; Jackson, J.; Walker, R. Late Cenozoic reorganization of the Arabia-Eurasia collision and the comparison of short-term and long-term deformation rates. *Tectonics* **2004**, *23*, 23. [[CrossRef](#)]
32. Regard, V.; Bellier, O.; Thomas, J.-C.; Abbassi, M.R.; Mercier, J.; Shabani, E.; Feghhi, K.; Soleymani, S. Accommodation of Arabia-Eurasia convergence in the Zagros-Makran transfer zone, SE Iran: A transition between collision and subduction through a young deforming system. *Tectonics* **2004**, *23*. [[CrossRef](#)]
33. Tatar, M.; Hatzfeld, D.; Ghafory-Ashtiany, M. Tectonics of the Central Zagros (Iran) deduced from microearthquake seismicity. *Geophys. J. Int.* **2004**, *156*, 255–266. [[CrossRef](#)]
34. Ghanbarian, M.A. Kinematic Analysis of the Tectonic Structures in the Hinterland of the Zagros Orogenic Belt, Iran. Ph.D. Thesis, Shiraz University, Shiraz, Iran, 2014. (In Persian).
35. Ghanbarian, M.A.; Sarkarinejad, K. Evidences of sinistral flow in the Zagros inclined transpression, Iran. In *Proceedings of the 2nd National Symposium on Tectonics of Iran*; Geological Survey of Iran: Tehran, Iran, 2014.
36. Ghanbarian, M.A.; Yassaghi, A.; Sadeghi Mazidi, M. Parallel transpressional deformation belts with different shear senses in the Zagros hinterland fold-and-thrust belt, Iran. In *Proceedings of the 2nd TRIGGER International Conference, Trans-Disciplinary Research on Iranian Geology, Geodynamics, Earthquakes and Resources*, Tehran, Iran, 12–16 November 2018; University of Tehran: Tehran, Iran, 2018.

37. Sadeghi Mazidi, M. *Paleo Stress Analysis of the Zagros Hinterland Fold-and-Thrust Belt in Bavanat to Shurjestan*; Shiraz University: Shiraz, Iran, 2019. (In Persian)
38. Bellahsen, N.; Faccenna, C.; Funicicello, F.; Daniel, J.; Jolivet, L. Why did Arabia separate from Africa? Insights from 3-D laboratory experiments. *Earth Planet. Sci. Lett.* **2003**, *216*, 365–381. [[CrossRef](#)]
39. Argus, D.F.; Gordon, R.G. No-net-rotation model of current plate velocities incorporating plate motion model NUVEL-1. *Geophys. Res. Lett.* **1991**, *18*, 2039–2042. [[CrossRef](#)]
40. Stocklin, J. Structural History and Tectonics of Iran: A Review. *AAPG Bull.* **1968**, *52*, 1229–1258. [[CrossRef](#)]
41. Sarkarinejad, K.; Ghanbarian, M.A. The Zagros hinterland fold-and-thrust belt in-sequence thrusting, Iran. *J. Asian Earth Sci.* **2014**, *85*, 66–79. [[CrossRef](#)]
42. Sarkarinejad, K. Tectonic finite strain analysis using Ghouri deformed conglomerate, Neyriz area, southwestern Iran. *Iran. J. Sci. Technol. Trans. B Eng.* **1999**, *23*, 352–363.
43. Ghanbarian, M.A.; Yassaghi, A. Structural and microstructural analyses of the deformation in the Faryadoun region, NE of the Zagros orogenic belt: Evidence for the occurrence of the sinistral shear. *Geosciences* **2020**, *30*, 243–252. [[CrossRef](#)]
44. Ghazi, J.M.; Moazzen, M. Geodynamic evolution of the Sanandaj-Sirjan Zone, Zagros Orogen, Iran. *Turk. J. Earth Sci.* **2015**, *24*, 513–528. [[CrossRef](#)]
45. Mohajjel, M. Structure and Tectonic Evolution of Palaeozoic-Mesozoic Rocks, Sanandaj-Sirjan Zone, Western Iran. Ph.D. Thesis, University of Wollongong, New South Wales, Australia, 1997.
46. Piryaei, A.; Reijmer, J.J.G.; van Buchem, F.S.P.; Yazdi-Moghadam, M.; Sadouni, J.; Danelian, T. The influence of Late Cretaceous tectonic processes on sedimentation patterns along the northeastern Arabian plate margin (Fars Province, SW Iran). *Geol. Soc. Lond. Spéc. Publ.* **2010**, *330*, 211–251. [[CrossRef](#)]
47. GSI. *Geological Map of Saadatshahr. Quadrangle 6650, 1:100 000*; Geological Survey of Iran: Tehran, Iran, 1996.
48. GSI. *Geological Map of Shiraz. Quadrangle 6549, 1:100 000*; Geological Survey of Iran: Tehran, Iran, 1999.
49. GSI. *Geological Map of Sivand. Quadrangle 6550, 1:100 000*; Geological Survey of Iran: Tehran, Iran, 2000.
50. GSI. *Geological Map of Dehbid. Quadrangle 6651, 1:100 000*; Geological Survey of Iran: Tehran, Iran, 2001.
51. GSI. *Geological Map of Eqlid. Quadrangle 6551, 1:100 000*; Geological Survey of Iran: Tehran, Iran, 1999.
52. GSI. *Geological Map of Abadeh. Quadrangle 6552, 1:100 000*; Geological Survey of Iran: Tehran, Iran, 2000.
53. GSI. *Geological Map of Shurjestan, Quadrangle 6452, 1:100 000*; Geological Survey of Iran: Tehran, Iran, 2001.
54. Goscombe, B.D.; Passchier, C.W.; Hand, M. Boudinage classification: End-member boudin types and modified boudin structures. *J. Struct. Geol.* **2004**, *26*, 739–763. [[CrossRef](#)]
55. Passchier, C.W.; Trouw, R.A. *Microtectonics*; Springer Science and Business Media: Berlin/Heidelberg, Germany, 2005.
56. Ramsay, J.G.; Huber, M.I. *The Techniques of Modern Structural Geology: Strain Analyses*; Academic Press: London, UK, 1983; Volume 1.
57. White, S. Large strain deformation: Report on a tectonic studies group discussion meeting held at Imperial College, London on 14 November 1979. *J. Struct. Geol.* **1979**, *1*, 333–339. [[CrossRef](#)]
58. Platt, J.; Vissers, R. Extensional structures in anisotropic rocks. *J. Struct. Geol.* **1980**, *2*, 397–410. [[CrossRef](#)]
59. Blenkinsop, T.G.; Treloar, P.J. Geometry, classification and kinematics of S-C and S-C' fabrics in the Mushandike area, Zimbabwe. *J. Struct. Geol.* **1995**, *17*, 397–408. [[CrossRef](#)]
60. Michibayashi, K.; Murakami, M. Development of a shear band cleavage as a result of strain partitioning. *J. Struct. Geol.* **2007**, *29*, 1070–1082. [[CrossRef](#)]
61. Tanner, P.G. A new model for the formation of a spaced crenulation (shear band) cleavage in the Dalradian rocks of the Tay Nappe, SW Highlands, Scotland. *J. Struct. Geol.* **2016**, *84*, 120–141. [[CrossRef](#)]
62. Berthé, D.; Choukroune, P.; Jegouzo, P. Orthogneiss, mylonite and non coaxial deformation of granites: The example of the South Armorican Shear Zone. *J. Struct. Geol.* **1979**, *1*, 31–42. [[CrossRef](#)]
63. Simpson, C.; Schmid, S.M. An evaluation of criteria to deduce the sense of movement in sheared rocks. *GSA Bull.* **1983**, *94*, 1281–1288. [[CrossRef](#)]
64. Woodcock, N.H.; Rickards, B. Transpressive duplex and flower structure: Dent Fault System, NW England. *J. Struct. Geol.* **2003**, *25*, 1981–1992. [[CrossRef](#)]
65. El-Wahed, M.A.A.; Kamh, S.Z. Pan-African dextral transpressive duplex and flower structure in the Central Eastern Desert of Egypt. *Gondwana Res.* **2010**, *18*, 315–336. [[CrossRef](#)]
66. Pavlis, T.L. Kinematic model for out-of-sequence thrusting: Motion of two ramp-flat faults and the production of upper plate duplex systems. *J. Struct. Geol.* **2013**, *51*, 132–143. [[CrossRef](#)]
67. Fujisaki, W.; Asanuma, H.; Suzuki, K.; Sawaki, Y.; Sakata, S.; Hirata, T.; Maruyama, S.; Windley, B.F. Ordovician ocean plate stratigraphy and thrust duplexes of the Ballantrae Complex, SW Scotland: Implications for the pelagic deposition rate and forearc accretion in the closing Iapetus Ocean. *Tectonophysics* **2015**, *662*, 312–327. [[CrossRef](#)]
68. Berglar, K.; Gaedicke, C.; Ladage, S.; Thöle, H. The Mentawai forearc sliver off Sumatra: A model for a strike-slip duplex at a regional scale. *Tectonophysics* **2017**, *710–711*, 225–231. [[CrossRef](#)]
69. Kleinschmidt, G.; Buggisch, W. Plate tectonic implications of the structure of the Shackleton Range, Antarctica. *Polarforschung* **1994**, *63*, 57–62. [[CrossRef](#)]

70. Kumar, P.S. An alternative kinematic interpretation of Thetis Boundary Shear Zone, Venus: Evidence for strike-slip ductile duplexes. *J. Geophys. Res. Space Phys.* **2005**, *110*, 110. [[CrossRef](#)]
71. Shalaby, A.; Stüwe, K.; Makroum, F.; Fritz, H.; Kebede, T.; Klötzli, U. The Wadi Mubarak belt, Eastern Desert of Egypt: A Neoproterozoic conjugate shear system in the Arabian-Nubian Shield. *Precambrian Res.* **2005**, *136*, 27–50. [[CrossRef](#)]
72. Agarwal, K.; Bali, R. Small-scale deformational structures as significant shear-sense indicators: An example from Almora Crystalline Zone, Kumaun Lesser Himalaya. *Earth Sci. India* **2008**, *1*, 119–124.
73. Marques, F.O.; Fonseca, P.D.; Lechmann, S.; Burg, J.-P.; Marques, A.S.; Andrade, A.J.; Alves, C. Boudinage in nature and experiment. *Tectonophysics* **2012**, *526–529*, 88–96. [[CrossRef](#)]
74. Aerden, D.G. The pyrite-type strain fringes from Lourdes (France): Indicators of Alpine thrust kinematics in the Pyrenees. *J. Struct. Geol.* **1996**, *18*, 75–91. [[CrossRef](#)]
75. Koehn, D.; Hilgers, C.; Bons, P.D.; Passchier, C.W.; Hilgers, C. Numerical simulation of fibre growth in antitaxial strain fringes. *J. Struct. Geol.* **2000**, *22*, 1311–1324. [[CrossRef](#)]
76. Lagoeiro, L.; Barbosa, P.F.; Fueten, F. Complex fringes around magnetite porphyroclasts: Growth and deformation history. *Tectonophysics* **2011**, *510*, 186–194. [[CrossRef](#)]
77. Holst, T.B.; Fossen, H. Strain distribution in a fold in the West Norwegian Caledonides. *J. Struct. Geol.* **1987**, *9*, 915–924. [[CrossRef](#)]
78. Zhang, J.; Xiao, W.; Han, C.; Ao, S.; Yuan, C.; Sun, M.; Geng, H.; Zhao, G.; Guo, Q.; Ma, C. Kinematics and age constraints of deformation in a Late Carboniferous accretionary complex in Western Junggar, NW China. *Gondwana Res.* **2011**, *19*, 958–974. [[CrossRef](#)]
79. Krabbendam, M.; Leslie, A. Folds with vergence opposite to the sense of shear. *J. Struct. Geol.* **1996**, *18*, 777–781. [[CrossRef](#)]
80. Liotta, D. D2 asymmetric folds and their vergence meaning in the Montagnola Senese metamorphic rocks (inner northern Apennines, central Italy). *J. Struct. Geol.* **2002**, *24*, 1479–1490. [[CrossRef](#)]
81. Ramsay, J.G.; Casey, M.; Kligfield, R. Role of shear in development of the Helvetic fold-thrust belt of Switzerland. *Geology* **1983**, *11*, 439–442. [[CrossRef](#)]
82. Little, T.A.; Miller, E.L.; Lee, J.; Law, R.D. Extensional origin of ductile fabrics in the Schist Belt, Central Brooks Range, Alaska—I. Geologic and structural studies. *J. Struct. Geol.* **1994**, *16*, 899–918. [[CrossRef](#)]
83. Ragan, D.M. Structures at the Base of an Ice Fall. *J. Geol.* **1969**, *77*, 647–667. [[CrossRef](#)]
84. Wynne-Edwards, H.R. Flow folding. *Am. J. Sci.* **1963**, *261*, 793–814. [[CrossRef](#)]
85. Fossen, H. *Structural Geology*; Cambridge University Press: Cambridge, UK, 2016; p. 510.
86. Sheikholeslami, M.; Pique, A.; Mobayen, P.; Sabzehei, M.; Bellon, H.; Emami, M.H. Tectono-metamorphic evolution of the Neyriz metamorphic complex, Quri-Kor-e-Sefid area (Sanandaj-Sirjan Zone, SW Iran). *J. Asian Earth Sci.* **2008**, *31*, 504–521. [[CrossRef](#)]
87. Zhang, B.; Zhang, J.; Zhong, D. Structure, kinematics and ages of transpression during strain-partitioning in the Chongshan shear zone, western Yunnan, China. *J. Struct. Geol.* **2010**, *32*, 445–463. [[CrossRef](#)]
88. Sarkarinejad, K.; Partabian, A.; Faghih, A. Variations in the kinematics of deformation along the Zagros inclined transpression zone, Iran: Implications for defining a curved inclined transpression zone. *J. Struct. Geol.* **2013**, *48*, 126–136. [[CrossRef](#)]
89. Javadi, H.R.; Ghassemi, M.R.; Shahpasandzadeh, M.; Guest, B.; Ashtiani, M.E.; Yassaghi, A.; Kouhpeyma, M. History of faulting on the Doruneh Fault System: Implications for the kinematic changes of the Central Iranian Microplate. *Geol. Mag.* **2013**, *150*, 651–672. [[CrossRef](#)]
90. Ghanbarian, M.A.; Sadeghi Mazidi, M. The effect of dextral Abarkuh Fault on the occurrence of sinistral top-to-the NW deformation in the Zagros Hinterland Fold-and-Thrust Belt, Iran. In Proceedings of the 3rd TRIGGER International Conference, Trans-Disciplinary Research on Iranian Geology, Geodynamics, Earthquakes and Resources, Zanjan, Iran, 8–10 October 2019.
91. Authemayou, C.; Chardon, D.; Bellier, O.; Malekzadeh, Z.; Shabanian, E.; Abbassi, M.R. Late Cenozoic partitioning of oblique plate convergence in the Zagros fold-and-thrust belt (Iran). *Tectonics* **2006**, *25*, 25. [[CrossRef](#)]
92. McQuarrie, N.; Stock, J.M.; Verdel, C.; Wernicke, B.P. Cenozoic evolution of Neotethys and implications for the causes of plate motions. *Geophys. Res. Lett.* **2003**, *30*. [[CrossRef](#)]
93. Klitgord, K.D.; Schouten, H. Plate kinematics of the central Atlantic. *West. N. Atl. Reg.* **1986**, 351–378. [[CrossRef](#)]
94. Srivastava, S.; Roest, W.; Kovacs, L.; Oakey, G.; Lévesque, S.; Verhoef, J.; Macnab, R. Motion of Iberia since the Late Jurassic: Results from detailed aeromagnetic measurements in the Newfoundland Basin. *Tectonophysics* **1990**, *184*, 229–260. [[CrossRef](#)]
95. Srivastava, S.P.; Tapscott, C.R.; Tucholke, B.E. Plate kinematics of the North Atlantic. *Geol. N. Am.* **1986**, *1000*, 379–404. [[CrossRef](#)]
96. Joffe, S.; Garfunkel, Z. Plate kinematics of the circum Red Sea—A re-evaluation. *Tectonophysics* **1987**, *141*, 5–22. [[CrossRef](#)]